Available online at www.sciencedirect.com
ScienceDirect
Computers and Mathematics with Applications 55 (2008) 1611–1619
An International Journal
computers & mathematics with applications
www.elsevier.com/locate/camwa

Study of axis-switching and stability of laminar rectangular jets using lattice Boltzmann method

Huidan Yu*, Sharath S. Girimaji

Aerospace Engineering Department, Texas A&M University, College Station, TX 77843-3141, USA

Abstract

We study stability characteristics and axis-switching behavior in low aspect-ratio (AR) laminar rectangular jets using lattice Boltzmann method. The objective of the study is to establish how the jet behavior changes with aspect ratio. Computations are performed with the D3Q19 multiple-relaxation-time lattice Boltzmann equation model. Simulations of three rectangular jets with $AR = 1$, 1.5 and 2 at four Reynolds numbers, 10, 100, 150, and 200, are performed. The main conclusions of this study are: (1) At low Reynolds numbers ($Re \leq 100$), the three jets are stable and no axis switching is observed. (2) At intermediate Reynolds numbers ($Re = 150$), axis switching is clearly evident. The square jet ($AR = 1$) exhibits 45° axis switching and tends to become unstable. The two rectangular jets continue to be stable and exhibit 90° axis switching. (3) At high Reynolds numbers ($Re \geq 200$), all three jets are unstable and the irregular instantaneous cross-section still shows evidence of axis switching. Instability originates near the jet orifice and then propagates down the stream. The physics underlying the 45° and 90° axis switching are examined.

Keywords: Lattice Boltzmann equation; Rectangular jet; Transition; Instability; Axis switching

1. Introduction

Jet flows have been the topic of extensive research in the past few decades due to their significance in practical applications. Non-circular jets have attracted increased attention owing to their superior mixing properties compared with round jets (cf. review [1] and references therein). Laboratory experiments [2–4] and numerical simulations [5–8] indicate a peculiar phenomenon called axis switching in rectangular turbulent jets (RTJ). Axis switching is characterized by the jet cross-section orientation rotation and typically occurs in low aspect-ratio (AR) RTJ flows [2,8–11]. This phenomenon is of interest both from fundamental physics and practical application points of view.

The present study is a part of an ongoing effort to investigate the flow physics of rectangular laminar jets (RLJ) and evaluates our ability to predict RTJs. In our previous works [8] we performed large eddy simulations (LES) of RTJs at high Reynolds numbers. The computed statistics agree reasonably well with experimental data quantitatively and qualitatively. That study also points out areas in which our physical understanding and predictive capabilities of RTJs need improvement. We seek to develop that improved understanding and modelling capabilities of RTJs by studying

* Corresponding address: CCS-2/CNLS, Los Alamos National Laboratory, USA.
E-mail addresses: hyu@lanl.gov (H. Yu), girimaji@aero.tamu.edu (S.S. Girimaji).

0898-1221/$ - see front matter © 2007 Elsevier Ltd. All rights reserved.
doi:10.1016/j.camwa.2007.08.011

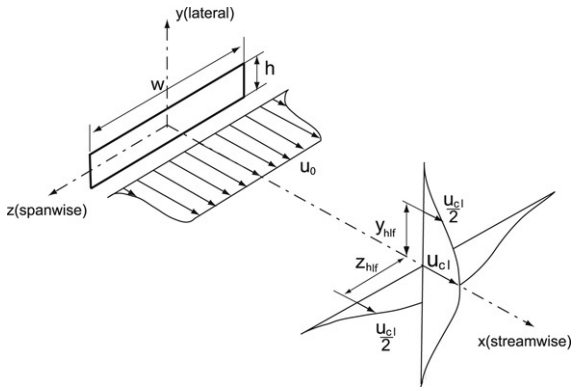

Fig. 1. Schematic configuration and coordinate system of the flow field.

instability characteristics of RLJs in great detail. Flow details that cannot be resolved in LES of high Reynolds number RTJs can be conveniently investigated in RLJs undergoing transition to turbulence. We have studied the behavior of a single RLJ of $AR = 1.5$ at different Reynolds numbers [12]. In this paper, our objective is to study how the stability and axis-switching characteristics of RLJs change with AR variation. We compare the behavior of jets of three different ARs.

We employ lattice Boltzmann method (LBM) as our numerical tool because of its physical simplicity and computational efficiency. In the past decade or so, LBM has been established as a physically accurate and computationally viable tool for simulating incompressible laminar and turbulent flows [8,13–15]. The computations are performed with the multiple-relaxation-time (MRT) lattice Boltzmann equation (LBE) model [16,17]. MRT-LBE has been demonstrated to be more accurate and stable than conventional LBE model [18,19] especially for high Reynolds number turbulent flows [8,20].

The remainder of this paper is organized as follows. Section 2 briefly formulates the numerical scheme — MRT-LBE. Computation results are presented in Section 3. Finally, we conclude with a brief summary in Section 4.

2. Numerical scheme and flow-field configuration

For our computations we use the D3Q19 MRT-LBE model, the details of which can be found elsewhere [17]. Here we only give a brief introduction.

In D3Q19 model, the discrete phase space is defined by a cubic lattice together with a set of discrete velocities $\{\vec{e}_\alpha|\alpha = 0, 1, \ldots, 18\}$. The 19 discrete velocities are $(0, 0, 0)$ for $\alpha = 0$; $(\pm1, 0, 0), (0, \pm1, 0), (0, 0, \pm1)$ for $\alpha = 1 - 6$, and $(\pm1, \pm1, 0), (\pm1, 0, \pm1), (0, \pm1, \pm1)$ for $\alpha = 7 - 18$. A set of velocity distribution functions $\{f_\alpha|\alpha = 0, 1, \ldots, 18\}$ is defined at each node $\vec{x}$ of the lattice. The MRT-LBE is

$$\mathbf{f}(\vec{x} + \vec{e}_\alpha \delta t, t + \delta t) - \mathbf{f}(\vec{x}, t) = -M^{-1}\hat{S}[\mathbf{m}(\vec{x}, t) - \mathbf{m}^{(eq)}(\vec{x}, t)]. \tag{1}$$

The bold-face symbol represents a column vector, e.g. $\mathbf{f} \equiv [f_0, f_1, \ldots, f_{18}]^{\mathrm{T}}$. Collision is executed in moment space spanned by the moments $\mathbf{m}$. It is transferred into velocity space $\mathbb{V}$ spanned by the distribution functions $\mathbf{f}$ through a linear mapping M: $\mathbf{m} = M\mathbf{f}$ or $\mathbf{f} = M^{-1}\mathbf{m}$ where M is a transformation matrix between two spaces. $\hat{S}$ is the diagonal collision matrix and $\mathbf{m}^{(eq)}$ are the corresponding equilibria of $\mathbf{m}$. The interested macroscopic quantities are obtained by $\rho = \sum_\alpha f_\alpha$ and $\rho\vec{u} = \sum_\alpha \vec{e}_\alpha f_\alpha$.

Fig. 1 shows the schematic flow-field configuration and coordinate system with a given uniform velocity profile at the jet exit slot. Three axes (x- streamwise, y- lateral, and z- spanwise), jet exit velocity u_0, centerline streamwise velocity u_{cl}, half-widths (y_{hlf}- lateral; z_{hlf}- spanwise), and jet geometry (width w, height h) are all shown.

The computational domain of the flow field is a $(W \times H \times L)$ channel. The inflow issues from a $(w \times h)$ orifice exit. This results in a jet of AR$\equiv w/h$. Jet exit has been simplified as a plane. We apply bounce-back boundary condition [21] at jet exit area ($x = 0$, $-w/2 \le z \le w/2$, and $-h/2 \le y \le h/2$) as follows

$$f_{\bar{\alpha}} = f_\alpha - 6w_\alpha \rho_b \vec{u}_b \cdot \vec{e}_\alpha, \tag{2}$$

Table 1
Parameter details of simulated jets

AR	$w \times h$	$W \times H \times L$	Jet exit grid size	Whole domain grid size
		$Re = 10, u_0 = 0.015$		
1.0	0.01×0.01	$0.1 \times 0.1 \times 0.1$	8×8	$80 \times 80 \times 160$
1.5	0.015×0.01	$0.15 \times 0.1 \times 0.2$	12×8	$120 \times 80 \times 160$
2.0	0.02×0.01	$0.2 \times 0.1 \times 0.2$	16×8	$160 \times 80 \times 160$
		$Re = 100, u_0 = 0.15$; $Re = 150, u_0 = 0.225$; $Re = 200, u_0 = 0.3$		
1.0	0.01×0.01	$0.075 \times 0.075 \times 0.2$	16×16	$120 \times 120 \times 320$
1.5	0.015×0.01	$0.11 \times 0.075 \times 0.2$	24×16	$180 \times 120 \times 320$
2.0	0.02×0.01	$0.15 \times 0.075 \times 0.2$	32×16	$240 \times 120 \times 320$

Units: length — (m), velocity — (ms^{-1}).

where $f_{\bar{\alpha}}$ is the distribution function of $\vec{e}_{\bar{\alpha}} := -\vec{e}_{\alpha}$, $w_0 = 1/3$, $w_{1-6} = 1/18$ and $w_{7-18} = 1/36$ are direction weight factors of D3Q19 lattice model. ρ_b and $\vec{u}_b$ are respectively the density and velocity at the boundary where the bounce-back collision occurs. The remainder of the jet exit plane is treated as a solid wall where the bounce-back equation (2) is still valid after setting $\vec{u}_b = 0$. Fully developed boundary condition is applied at outflow ($x = L$) [20]. Initially, the velocity field is $\vec{u} = 0$ everywhere in the computational domain except the jet exit area. The initial density field is uniform as ρ_0. We assume $\rho_b = \rho_0$.

The computational parameters for the three simulated jets are listed in Table 1. The Reynolds number (Re) is based on h, u_0, and ν. We set $u_0 = 0.1$ in lattice unit. The values for the relaxation rates are chosen as suggested by Ref. [17].

3. Simulation results

We examine the shape of the half-width streamwise velocity contour (HWSVC) and secondary-motion vector field at various downstream planes to monitor axis switching and onset of instability. The HWSVC at a given downstream plane (x-plane) is the contour of the points (y_{hlf}, z_{hlf}) on the plane at which the streamwise velocity is one-half of the centerline streamwise velocity:

$$u(x, y_{hlf}, z_{hlf}) = \frac{1}{2} u_{cl}(x, 0, 0) \tag{3}$$

The HWSVC is a direct measure of the level of mixing. Fast spreading of HWSVC indicates rapid entrainment and mixing. The physics of entrainment and HWSVC evolution can be understood by examining the secondary flow: i.e., flow on the transverse plane (y, z) normal to the primary flow direction (x). The results are presented in two parts: axis switching and instability onset. In all the figures the dashed line represents the orifice shape which is also the initial jet shape.

3.1. Axis-switching behavior

At relatively low Re numbers ($\leq$100), HWSVCs of all jets tend to be circular and no axis switching occurs, as seen in Fig. 2. In the square jet case this indicates that the contour changes more rapidly along the four axes than along the diagonals. Thus mixing is more rapid along the axes than along the diagonals. In the rectangular jets the ultimate circular HWSVC indicates that the mixing is more rapid along the minor axis than along the major axis. These fundamental tendencies are important to note as they form the basis of axis switching at higher Reynolds numbers.

At $Re = 150$, axis switching occurs in all the three jets but the details of the phenomena depend on the aspect ratio. The square jet exhibits 45° axis switching as shown in Fig. 3(a). The jet cross-section shape rotates from y–z plane (dashed line) to an orientation parallel to the diagonal direction of the jet exit shape. However, in Fig. 3(b), the RLJ with $AR = 2$ exhibits a 90° axis switching displaying the change in the orientation of its major axis from initial spanwise to lateral direction. We examine in more detail the axis-switching process in $AR = 1.5$ jet (Fig. 4) which also exhibits 90° axis switching. Fig. 4 shows that the jet spreads from the rectangular shape (dashed line) with the major axis on spanwise direction near the jet orifice (at $x = h$ and $3h$) through an elliptical shape with the major

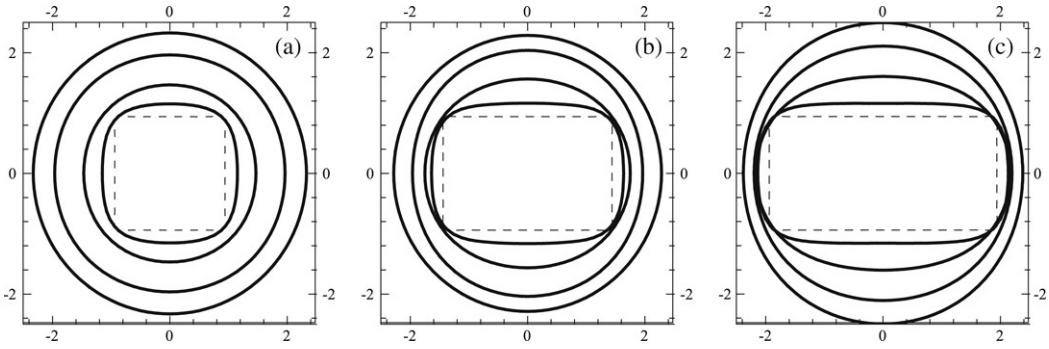

Fig. 2. Evolution of HWSVCs downstream (outward) at $Re = 100$. (a) $AR = 1$; (b) $AR = 1.5$; (c) $AR = 2$.

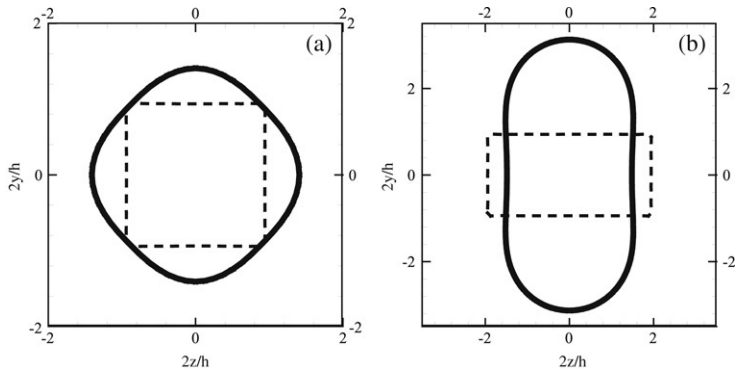

Fig. 3. Axis-switching behavior of RLJs on transverse planes at $Re = 150$. (a) $AR = 1$, $x = 3h$; (b) $AR = 2$, $x = 7h$.

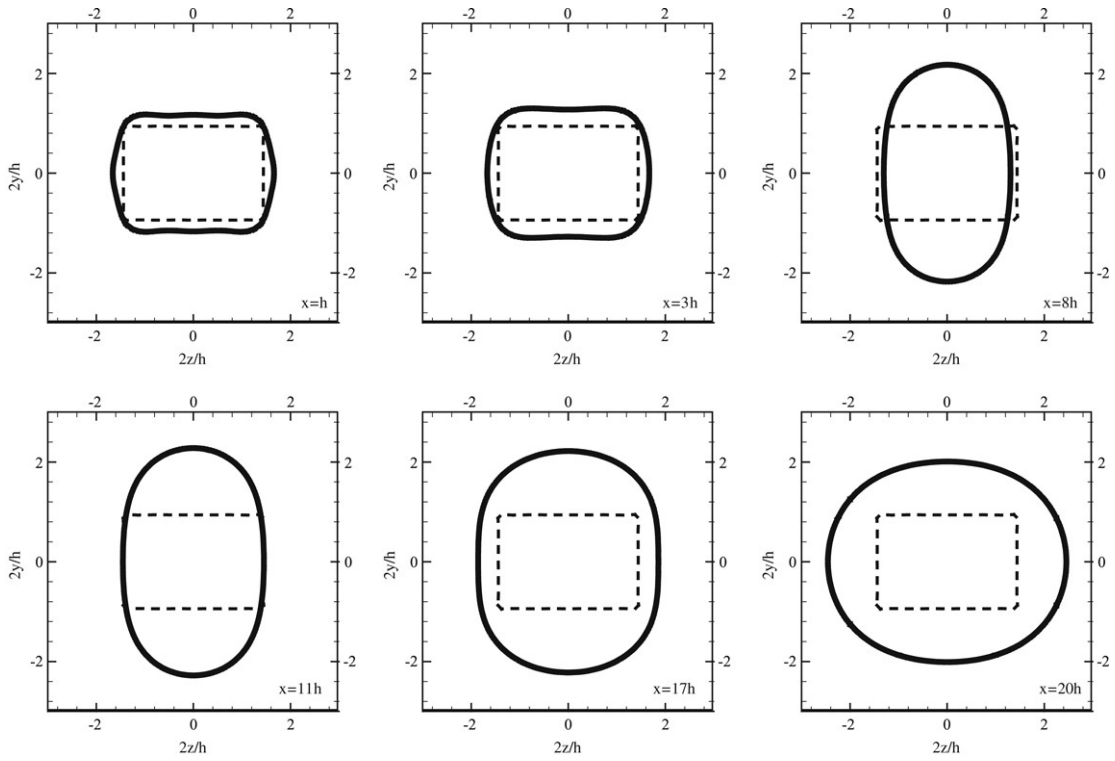

Fig. 4. 90° axis switching of RLJ ($AR = 1.5$) on transverse planes at $Re = 150$.

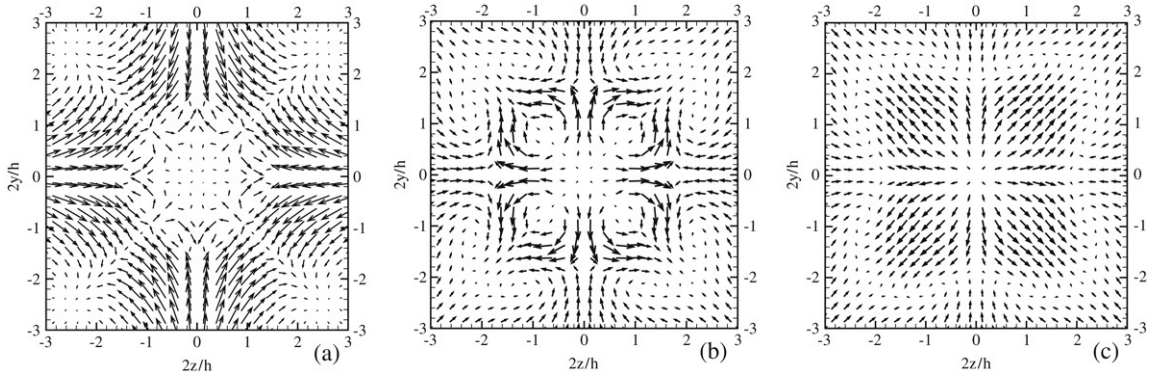

Fig. 5. Transverse velocity planes of the square jet at $Re = 150$. (a) $x = h$; (b) $x = 3h$; (c) $x = 5h$.

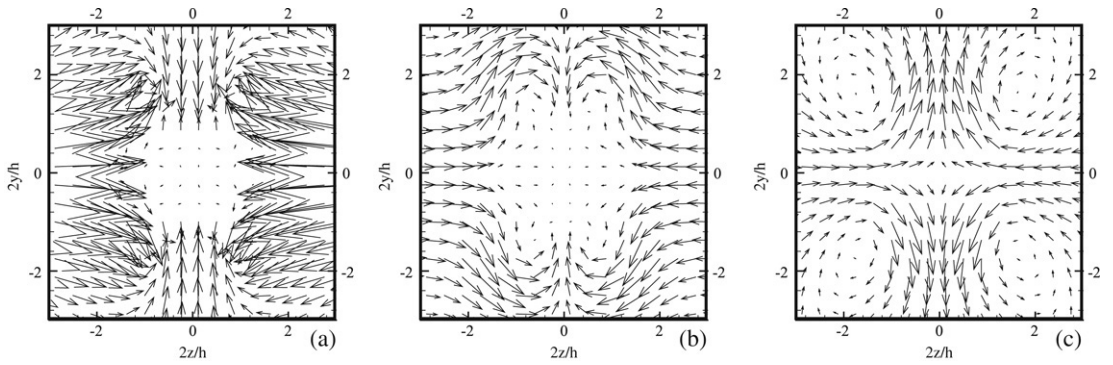

Fig. 6. Transverse velocity planes of RLJ ($AR = 1.5$) at $Re = 150$. (a) $x = h$; (b) $x = 3h$; (c) $x = 5h$.

axis on lateral direction in the intermediate planes (at $x = 8h$, $11h$, and $17h$) to an oval further down the stream (at $x = 20h$) where the major axis returns back to the spanwise direction. But the aspect ratio on the return to the original orientation is smaller than the initial ratio. As the jet moves further down, the switching cycle repeats itself with the aspect ratio approaching unity and HWSVC gradually becomes axisymmetric (circular).

In order to investigate the underlying mechanism of axis-switching behavior, we next examine the secondary or transverse velocity vector fields (u_y and u_z) at different downstream locations in Fig. 5 for the square jet and Fig. 6 for the RLJ with $AR = 1.5$.

Square jet. Adjacent to the jet exit ($x = h$), the secondary flow is weak and radially inward along the axes; it is strong and tangential closer to the corners. Thus, there is some entrainment of the ambient flow into the jet core along the axes and not much entrainment at the corners. This explains why the corners of the HWSVC do not show much movement. A little downstream ($x = 3h$), there is a strong outflow from the jet center along the axes. At this time the flow along the diagonal is inward and weak. The secondary flow pattern suggests the presence of eight vortices, two in each quadrant of the jet. The vortices in each quadrant are counter rotating. The rotation is such that the velocities (nearly) cancel along the diagonals and are augmented along the axis. This explains the observed strong outflow along the axes and weak inflow along the diagonals at $x = 3h$. The strong axial outflow carries high momentum jet fluid to outside the initial jet core along the transverse axes. As the diagonal inflow is weak, there is no significant momentum transport in that direction. Thus, the HWSVC stretches along the axes and stays nearly the same at the corners leading to axis switching (as seen in Fig. 3(a)). After the first switch, the diagonal and axes directions are reversed. Past $x = 3h$, the second-switching process is initiated. At $x = 5h$ (Fig. 5(c)), we can see that strong outflow along the new axial direction (old diagonal direction) and weak flow along the new diagonal direction (old axial direction). This flow pattern results in axis being switched back to the old orientation. Thus, one cycle of axis switching back and forth is completed by $x = 6h$. This switching back and forth continues until the flow becomes axisymmetric as mentioned before.

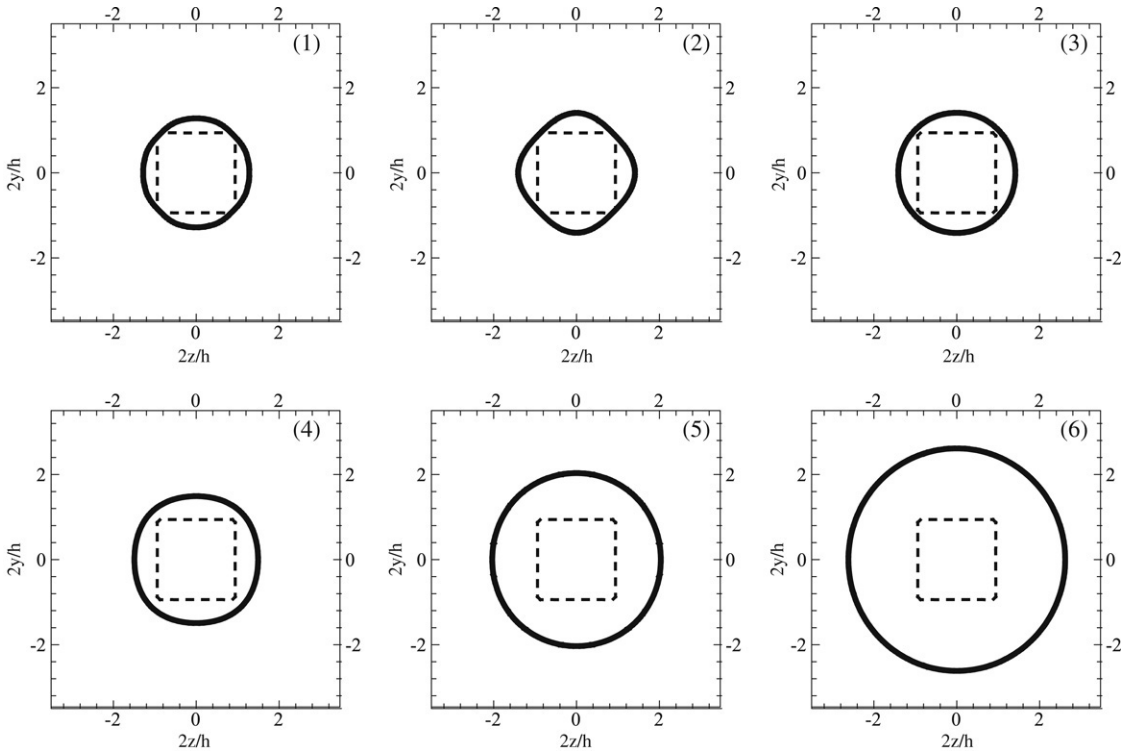

Fig. 7. HWSVCs of the square jet at $Re = 150$ at an early time instant ($t = 1.68$ s). (1) $x = h$; (2) $x = 2h$; (3) $x = 5h$; (4) $x = 8h$; (5) $x = 13h$; (6) $x = 15h$.

Rectangular jets. The flow pattern in $AR = 1.5$ case is somewhat different (Fig. 6). Initially, at $x = h$, the flow comes towards the center along the axes from all four directions as in the case of the square jet. But one significant difference from the square jet case is that the flow in the spanwise direction is stronger than in lateral direction. The flow pattern at $x = 3h$ is similar to that at $x = h$ with the exception that the velocity magnitudes are much smaller in all directions. The flow pattern at $x = 5h$ reveals the presence of four vortices, one in each quadrant. This is a significant departure from the square jet case. The rotation of the four vortices are such that the secondary flow is into the jet along the spanwise direction and out of the jet along the lateral direction. The inflow brings low momentum ambient fluid into the jet core along the spanwise direction. This results in the HWSVC moving into the original jet core along the spanwise axis. The lateral outflow takes high momentum jet-core fluid to the outside. This results in the HWSVC moving outwards in the lateral direction. The net result is the switching of the axes at $x = 7h$ as seen in Fig. 3(b). The second switching cycle is initiated beyond this downstream location.

In summary, the 90° axis switching in rectangular jet takes much longer ($x = 7h$) than the 45° axis switching in square jet. Indeed, one cycle of axis switching (two switches) is complete in a square jet by $x = 6h$, before a single switch is complete in the rectangular jet.

3.2. Instability onset

At low Reynolds numbers ($Re \leq 100$) the flow fields of the three jets are stable and attain steady state quickly as shown in Fig. 2. At $Re = 150$, two RLJs with $AR = 1.5$ and 2 are still stable and laminar. The flow structure of RLJ with $AR = 1.5$ can be found in our previous work [12]. We now turn our attention to the square jet. At early times, the square jet appears quite stable (Fig. 7). With passage of time (Fig. 8) instabilities start appearing close to the jet exit ($x \leq 2h$). Farther downstream the flow appears quite stable. As more time passes, this instability propagates downstream rendering the whole jet unstable (Fig. 9). Despite the instability, the axis switching can still be seen in these figures.

As the *Re* number increases, even the rectangular jets become unstable. Fig. 10 shows the irregular flow structures of the RLJ with $AR = 2$ at $Re = 200$. Careful examination once again reveals that the instability is initiated at the jet

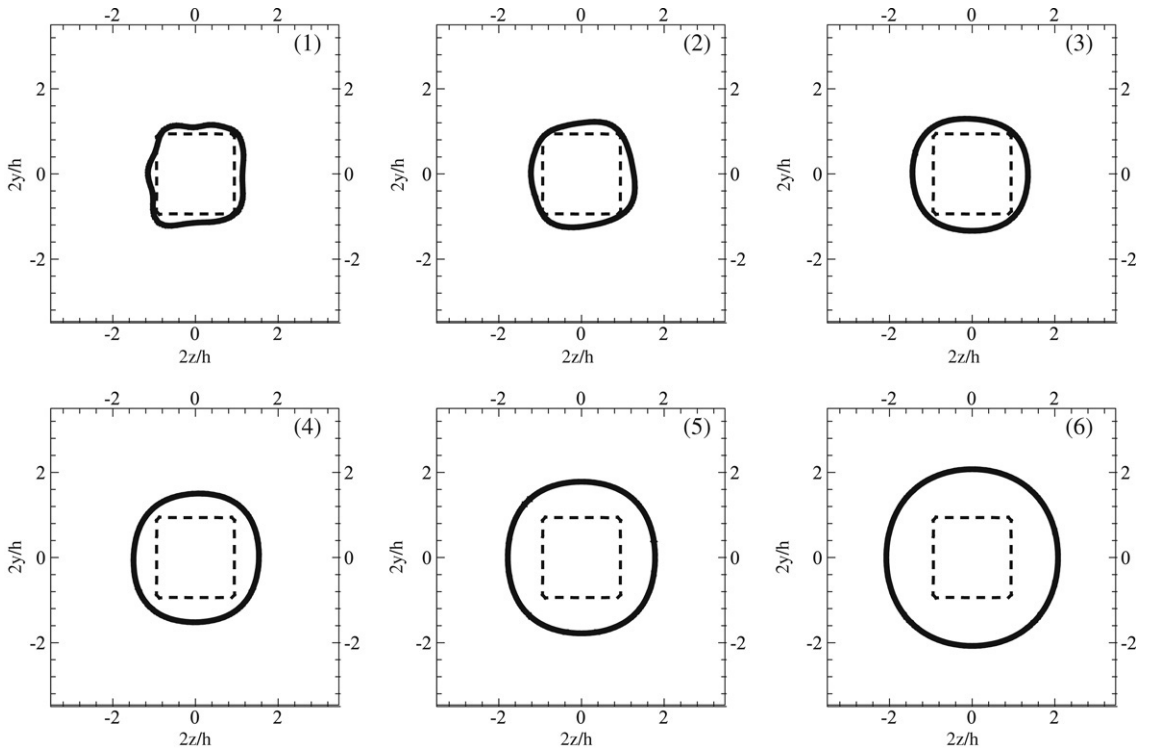

Fig. 8. HWSVCs of the square jet at $Re = 150$ at an intermediate time instant ($t = 3.93$ s). (1) $x = h$; (2) $x = 2h$; (3) $x = 5h$; (4) $x = 8h$; (5) $x = 13h$; (6) $x = 15h$.

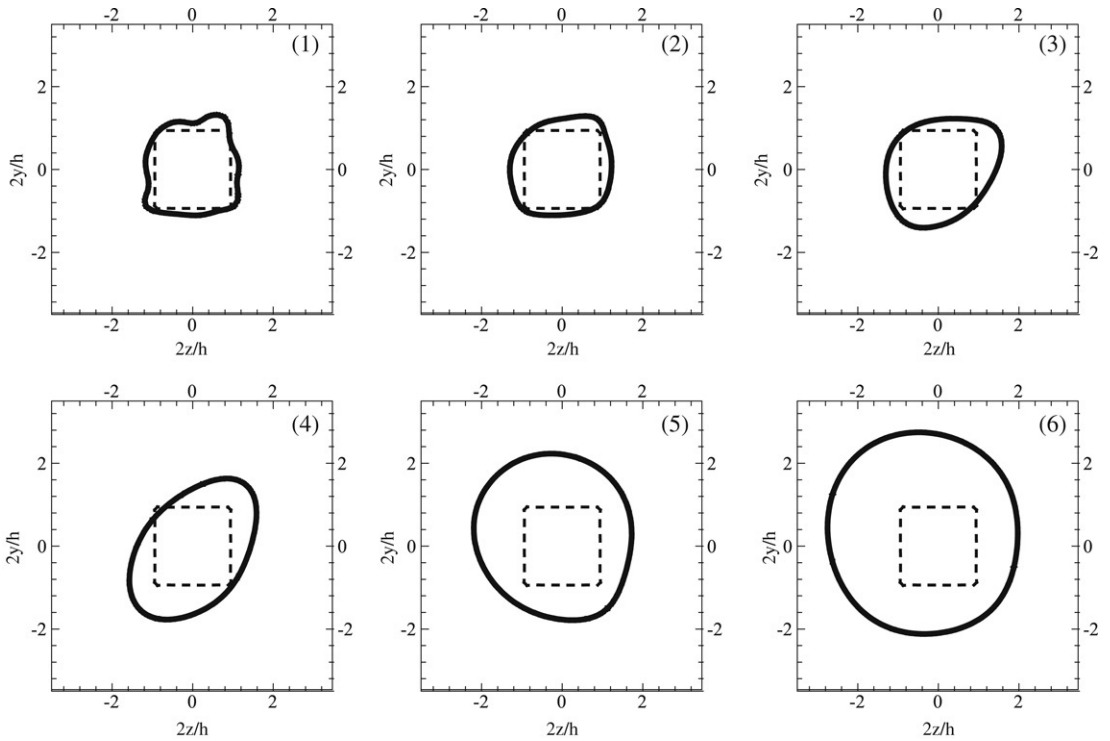

Fig. 9. HWSVCs of the square jet at $Re = 150$ at a late time instant ($t = 6.16$ s). (1) $x = h$; (2) $x = 2h$; (3) $x = 5h$; (4) $x = 8h$; (5) $x = 13h$; (6) $x = 15h$.

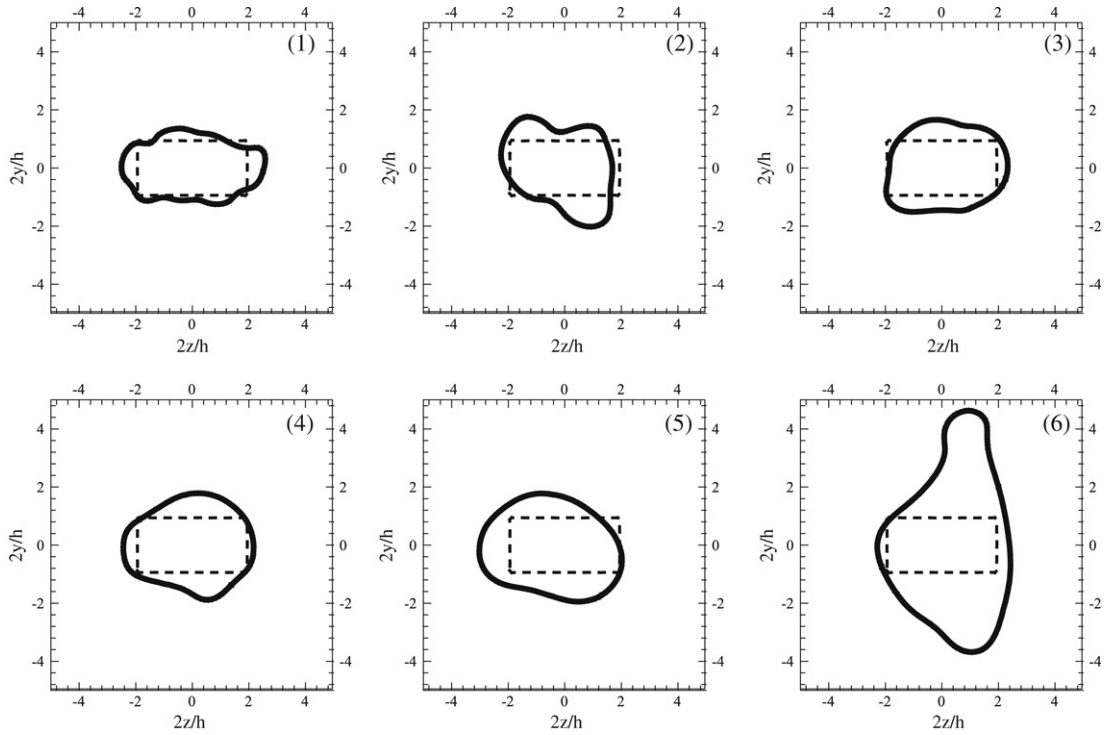

Fig. 10. HWSVCs of RLJ ($AR = 2$) at $Re = 200$ at a late time instant ($t = 5.04$ s). (1) $x = 2h$; (2) $x = 4h$; (3) $x = 6h$; (4) $x = 7h$; (5) $x = 8h$; (6) $x = 10h$.

exit and then propagates downstream, as was seen in the square jet. Again, the 90° axis switching is still roughly seen in Fig. 10.

In summary, it is clear that square jet becomes unstable at a lower Reynolds number than rectangular jets. The reason for this is quite simple. With eight streamwise vortices, the square jet experiences a higher degree of unsteadiness than a rectangular jet as was demonstrated previously. Due to inherent unsteadiness, it appears more prone to instabilities.

4. Conclusion

This work simulates the flow structure of three jets with $AR = 1$, 1.5, and 2. At relatively low Re numbers (10,100), three jets are laminar and no axis switching occurs. At $Re = 150$, two RLJs with $AR = 1.5$ and 2 are still laminar and stable and 90° axis switching is seen. However the square jet exhibits a 45° axis switching and tends to become unstable. At higher Re number (200), all three jets are unstable and axis switching can still be observed in the instantaneous profiles.

Our findings are summarized as follows:

(1) Although axis switching occurs in both square and rectangular jets, the former switches 45° while the latter 90°.
(2) The secondary flow pattern in the square jet reveals eight vortices. The rectangular jet flow field is made up of only four vortices.
(3) Axis switching of square jet happens closer to the jet exit than in the case of rectangular jets. Square jets are also less stable.
(4) Jet instability is initiated at the jet exit area and propagates downstream.

Acknowledgment

Part of this work was supported by the United States Air Force Office for Scientific Research under Grant No. F49620-01-1-0142.

References

[1] E.J. Gutmark, F.F. Grinstein, Annu. Rev. Fluid Mech. 31 (1999) 239.
[2] Y. Tsuchiya, C. Horikoshi, T. Sato, Exp. Fluids 4 (1986) 197.
[3] W.R. Quinn, Exp. Therm. Fluid Sci. 5 (1992) 203.
[4] W.R. Quinn, Aeronaut. J. 2110 (1995) 337.
[5] B. Rembold, N.A. Adams, L. Kleiser, Int. J. Heat Fluid Flow 23 (2002) 547.
[6] R.V. Wilson, A.O. Demuren, J. Fluids Eng. 120 (1998) 285.
[7] R.S. Miller, C.K. Madnia, P. Givi, Comput. Fluids 24 (1995) 1.
[8] H. Yu, S.S. Girimaji, Phys. Fluids 17 (2005) 125106.
[9] G.F. Marsters, J. Fotheringham, Aeron. Q. 31 (1980) 285.
[10] G.F. Marsters, AIAA J. 19 (1981) 148.
[11] W.R. Quinn, AIAA J. 32 (1994) 547.
[12] H. Yu, S.S. Girimaji, Physica A 362 (2006) 151.
[13] S. Chen, G. Doolen, Annu. Rev. Fluid Mech. 30 (1998) 329.
[14] L.S. Luo, in: J.H. Wu, Z.J. Zhu (Eds.), Proc. Inter. Conf. Appl. Comp. Fluid Dyn., Beijing, 2000, p. 52.
[15] D. Yu, R. Mei, L.S. Luo, W. Shyy, Prog. Aerosp. Sci. 39 (2003) 329.
[16] D. d'Humières, Rarefied Gas Dynamics: Theory and Simulations, in: B.D. Shizgal, D.P. Weaver (Eds.), Prog. Aeronaut. Astronaut., vol. 159, 1992, p. 450.
[17] D. d'Humières, I. Ginzburg, M. Krafczyk, P. Lallemand, L.-S. Luo, Phil. Trans. R. Soc. London A 360 (2002) 437–451.
[18] H. Chen, S. Chen, H.W. Matthaeus, Phys. Rev. A 45 (1992) R5339.
[19] Y.H. Qian, D. d'Humières, P. Lallemand, Europhys. Lett. 17 (1992) 479.
[20] H. Yu, L.-S. Luo, S.S. Girimaji, Comput. Fluids 35 (2006) 957–965.
[21] L.-S. Luo, Phys. Rev. E 62 (2000) 4982–4996.